Electronic Supplementary Material (ESI) for Nanoscale.

Supporting Information

Borazatruxenes as precursors for hybrid C-BN 2D molecular networks

Anamaria Trandafir[1,2,3,4], G. Dan Pantoș[2,3], and Adelina Ilie[1,3,4*]

[1] Department of Physics, University of Bath, Bath, UK
[2] Department of Chemistry, University of Bath, Bath, UK
[3] Centre for Graphene Science, University of Bath, Bath, UK
[4] Centre for Nanoscience and Nanotechnology, University of Bath, Bath, UK

*Corresponding author: a.ilie@bath.ac.uk

1. Single molecules on Au(111)

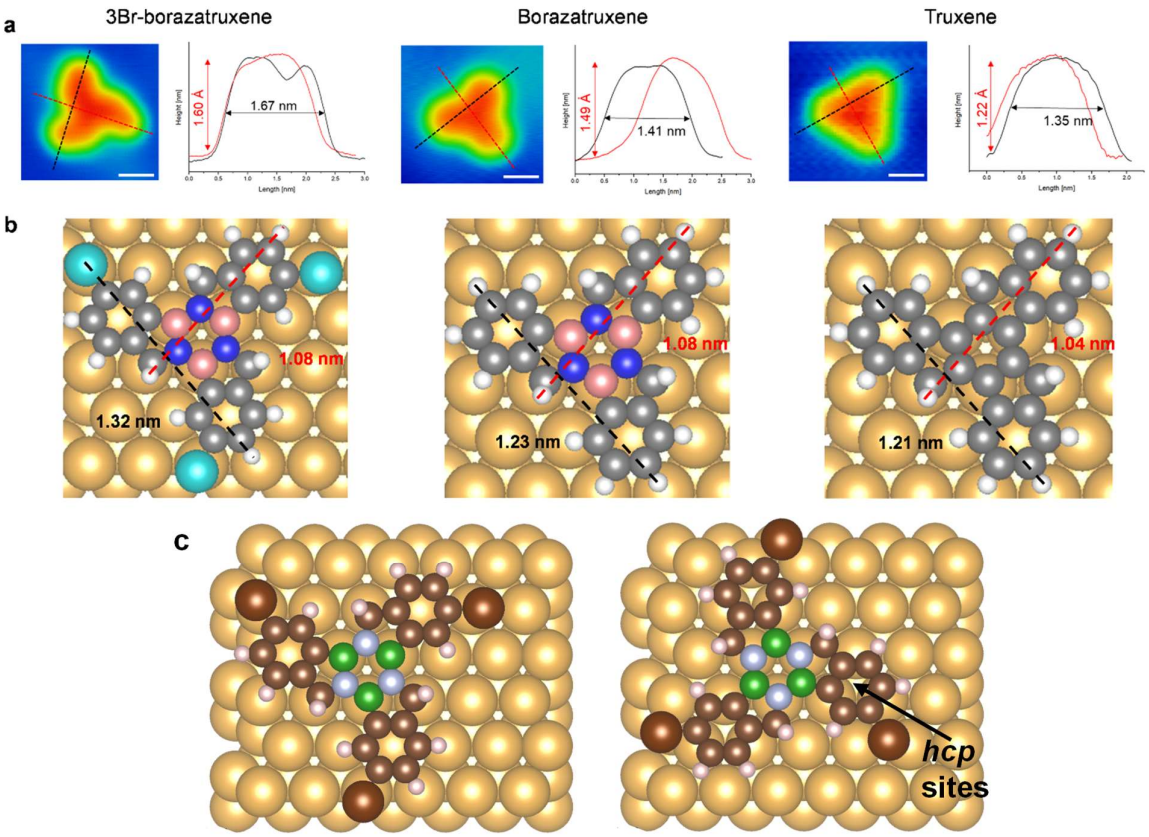

Figure S1. **Geometry comparison between 3Br-borazatruxene, borazatruxene and truxene.** (a) Experimental line profiles of all three molecules showing their lateral size at FWHM and apparent height in STM z images. Scanning parameters: 3Br-borazatruxene, -2V, 0.4 nA; borazatruxene, -2V, 0.5 nA; and truxene, -2V, 0.3 nA. Scale bar is 0.5 nm. (b) Lateral size of the optimized geometry of precursors on Au(111) (at PBE+D3 level), measured from the center-to-center of atomic radii. Color coding: N, blue; B, pink; Br, cyan; C, grey; H, white. Molecule sizes were calculated from these structural models by adding van der Waals radii to the center-to-center distances; this results in dimensions that correspond well to the experimental profiles at FWHM from (a). (c) Left image shows an *R* molecule in its optimized position relative to the Au(111) surface: this orientation is labelled as A, corresponding to Figure 1. Right image shows this molecule rotated by 60°, corresponding to orientation B: this orientation is not equivalent relative to the Au(111) surface to A due to the molecule's chirality. Indeed, in orientation B, N atoms are on top of Au atoms, B atoms are above the *hcp* sites of the Au(111) surface, CH_2 groups are above the *hcp* sites, and the aromatic C rings surround the *hcp* sites; while in orientation A, B atoms are on top of Au atoms, N atoms are above the *hcp* sites, CH_2 groups are above the Au atoms, while the aromatic C rings surround Au atoms. The environment of the Br atoms is also different in the two molecular orientations. This non-equivalence explains why only one orientation is observed on Au(111) for the 3Br-borazatruxene monomer.

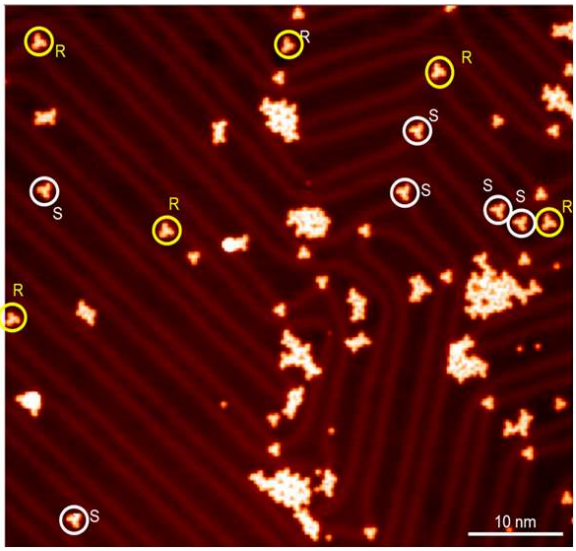

Figure S2: **3Br-borazatruxene enantiomers of differing chirality are adsorbed in a single conformation on the Au(111) surface, which depends on their chirality.** Constant current STM z image of low coverage of 3Br-borazatruxene on Au(111) showing that each enantiomer (R or S) adsorbs in a single conformation, labelled A in the main text. Tunneling parameters: -2V, 0.3 nA.

2. Structure optimization of 3Br-borazatruxene configurations in vacuum

a

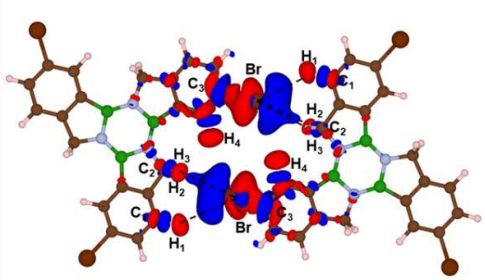

	Distances (Å)
$Br\text{-}H_1$	3.24
$Br\text{-}C_1$	4.13
$Br\text{-}H_2$	3.20
$Br\text{-}H_3$	3.36
$Br\text{-}H_4$	3.57
$Br\text{-}C_2$	3.75
	Angles (°)
$C_2\text{-}H_3\cdots Br$	101.8
$C_2\text{-}H_2\cdots Br$	111.7
$C_1\text{-}H_1\cdots Br$	138.4

b

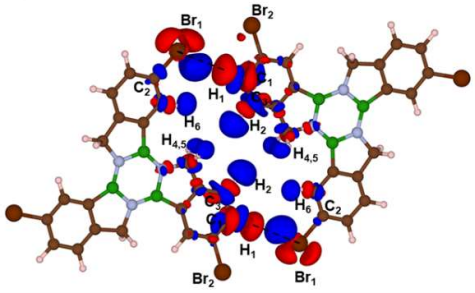

	Distances (Å)
$Br_1\text{-}H_1$	3.04
$Br_1\text{-}C_1$	4.11
$Br_1\text{-}Br_2$	4.37
$H_1\text{-}H_6$	3.00
$H_2\text{-}H_{4,5}$	3.06
$H_2\text{-}H_6$	3.32
	Angles (°)
$C_2\text{-}Br_1\cdots H_1$	106.5
$C_2\text{-}Br_1\cdots Br_2$	149.0
$C_2\text{-}H_6\cdots H_2$	135.2
$C_3\text{-}H_2\cdots H_6$	120.5
$C_3\text{-}H_2\cdots H_4$	160.5
$C_3\text{-}H_2\cdots H_5$	159.0

c

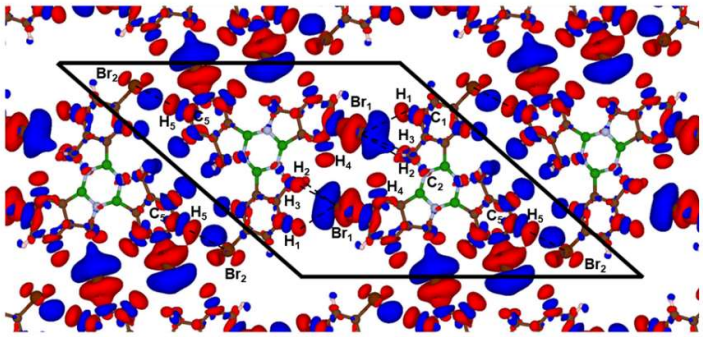

	Distances (Å)
$Br_1\text{-}H_1$	3.37
$Br_1\text{-}H_2$	3.26
$Br_1\text{-}H_3$	3.36
$Br_1\text{-}C_1$	4.13
$Br_1\text{-}C_2$	3.77
$Br_1\text{-}H_4$	3.63
$Br_2\text{-}H_5$	3.03
$Br_2\text{-}C_5$	4.10
	Angles (°)
$C_2\text{-}H_3\cdots Br_1$	97.9
$C_2\text{-}H_2\cdots Br_1$	115.4
$C_1\text{-}H_1\cdots Br_1$	138.8
$C_5\text{-}H_5\cdots Br_2$	167.7

d

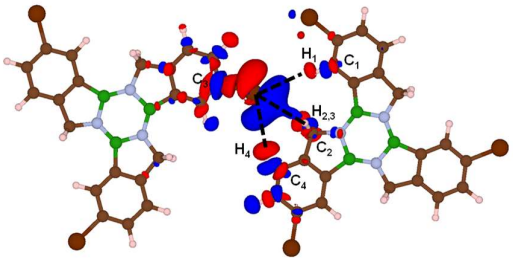

	Distances (Å)
Br-H_1	3.33
Br-C_1	4.42
Br-H_2	3.19
Br-H_3	3.30
Br-H_4	3.41
Br-C_2	3.73
Br-C_4	4.27
	Angles (°)
C_2-H_3···Br	104.37
C_2-H_2···Br	111.13
C_1-H_1···Br	173.25
C_4-H_4···Br	136.78

Figure S3. **Various assemblies of 3Br-borazatruxene: DFT-optimized structures, computed interatomic distances and angles.** (a) Type 1 homodimer, observed experimentally, contains two tri-furcated H bonds. (b) "Tip-to-tip" dimer, not observed experimentally, contains two single H bonds. (c) The low symmetry, 2D network entails both types of dimeric interactions seen in (a) and (b) in the unit cell. Tables tabulate various interatomic distances and angles, complementing the information from Figure 3. (d) A-A heterodimer (as shown in Figure 1d). The Br-C_1 and Br-C_4 distances are similar, so the H bond is shared between all 4 H atoms (labelled 1 to 4). There is a higher electron density between Br and H_4 compared to the homodimer. The binding energy per monomer is -12.87 meV, less than half the binding energy of the homodimer.

In all situations, shorter interatomic distances, and angles approaching 180° indicate strong, directional interactions. All charge density difference maps are plotted at $\rho(r)=0.00015$ e/bohr^3 isosurface value. Excess of electrons, blue; deficit of electrons, red.

3. Edges of 3Br-borazatruxene homochiral domains on Au(111)

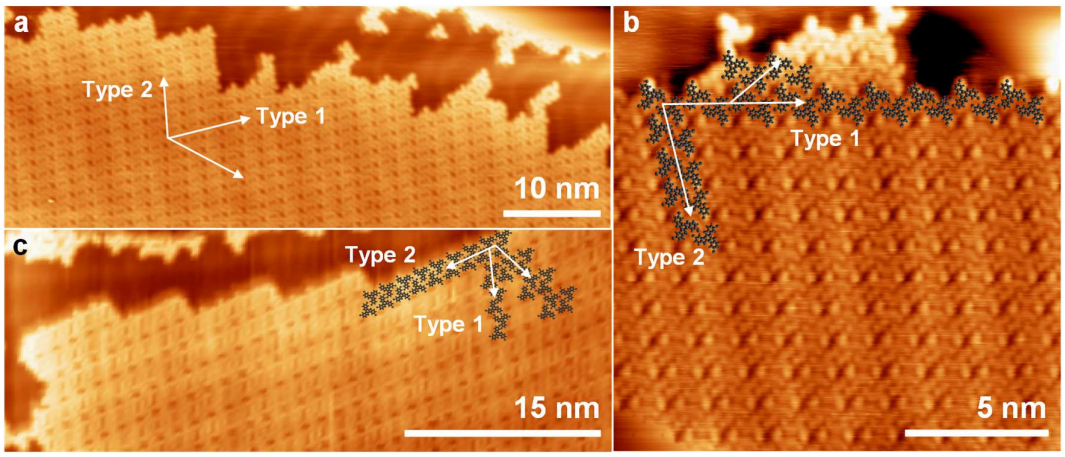

Figure S4. STM z images of domains of low-symmetry, 3Br-borazatruxene 2D molecular network on Au(111) showing the formation of network edges: (a-b) along type 1, and (c) type 2 chain bonding directions, respectively. The crystallographic axes of this network are defined in a manner consistent with Figure 2 main text. Superimposed are shown pairs of homodimers that are the building blocks of the domains. Domains are enantiopure.

4. Structure optimization of low symmetry, 3Br-borazatruxene 2D network on Au(111

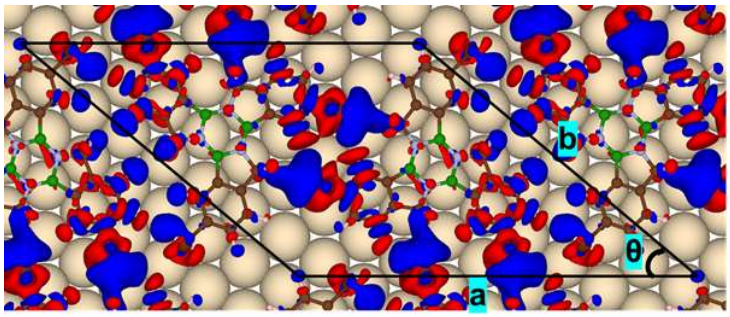

Optimized geometry of 2D network on Au	
a	2.34 nm
b	2.17 nm
θ	39.88°

	Distances (Å)
Br_1-H_1	3.70
Br_1-H_2	2.95
Br_1-H_3	3.07
Br_1-C_1	4.45
Br_1-C_2	3.52
Br_1-H_4	2.81
Br_2-H_5	3.00
Br_2-C_5	4.07
	Angles (°)
C_2-H_3···Br_1	104.88
C_2-H_2···Br_1	111.76
C_1-H_1···Br_1	127.11
C_4-H_4···Br_1	177.74
C_5-H_5···Br_2	167.82

Figure S5 Low symmetry, 3Br-borazatruxene 2D H-bonded network on Au(111): DFT-optimized structure and charge density difference map (plotted for ρ(r)=0.00015 e/bohr^3 isovalue) showing the type of interaction within the unit cell. Computed interatomic distances and angles show a stronger binding within the dimer than in vacuum. The atomic numbering in the figure has been omitted for clarity, but refer to the same atomic species as in Figure S3. Excess of electrons: blue, deficit of electrons: red.

5. Alternative 3Br-borazatruxene 2D networks, computations in vacuum

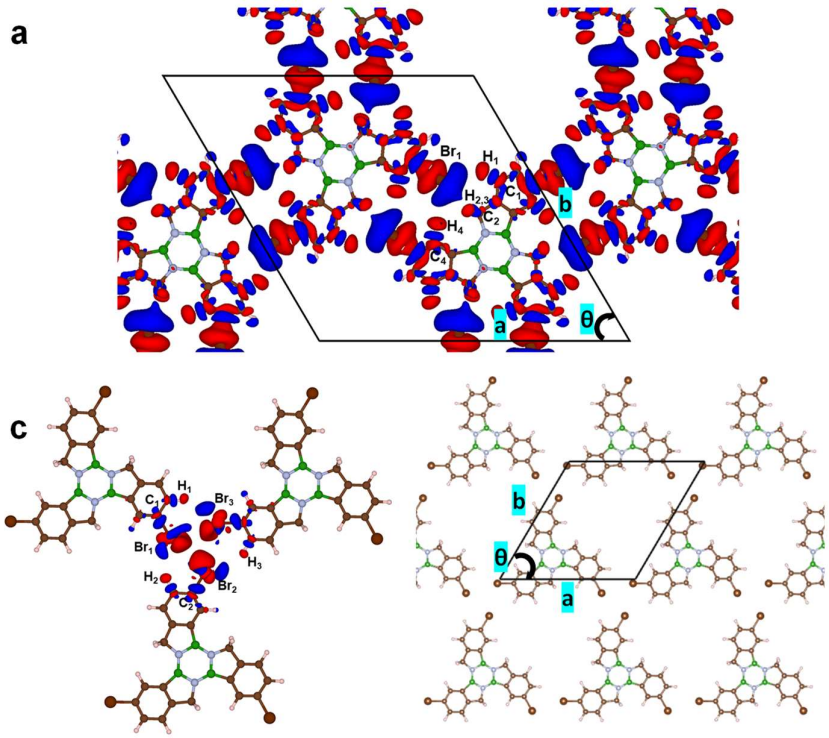

b

	Distances (Å)
Br_1-H_1	3.27
Br_1-H_2	3.18
Br_1-H_3	3.22
Br_1-C_1	4.14
Br_1-C_2	3.68
Br_1-C_4	4.41
Br_1-H_4	3.40
	Angles (°)
C_1-H_1···Br_1	137.2
C_4-H_4···Br_1	178.8
C_2-H_2···Br_1	107.9
C_2-H_3···Br_1	105.8

d

	Distances (Å)
Br_1-H_2	3.45
Br_1-Br_2	3.92
	Angles (°)
C_1-Br_1···Br_2	154.7
C_2-Br_2···Br_1	102.3
C_1-Br_1···H_2	140.9

e

	C_6-symmetry H-bonded 2D network	C_3-symmetry halogen-halogen 2D network
a	2.16 nm	1.57 nm
b	2.15 nm	1.59 nm
θ	59.51°	59.48°

Figure S6 Alternative 2D assemblies of 3Br-Borazatruxene. C_6-symmetry 3Br-Borazatruxene H-bonded network. (a) Charge density difference map (CDD), $\Delta\rho(r) = \rho_{network} - \sum_{i=1}^{2} \rho_{monomer_i}$, for Δρ(r)=0.00015 e/bohr^3 isovalue. (b) Geometrical parameters of the optimized structure, showing the double trifurcated H

bond character occurring between adjacent monomers within the network. **C_3-symmetry assembly *via* type II halogen-halogen interactions.** (c) Left: CDD map for a trimer assembly of 3Br-Borazatruxene, calculated as $\Delta\rho(r) = \rho_{trimer} - \sum_{i=1}^{3} \rho_{monomer_i}$; excess of electrons, blue; deficit of electrons, red. The 3Br-Borazatruxene trimer geometry was selected from the optimized geometry of the corresponding bespoke 2D network shown on the right. (d) Optimized geometrical parameters of the C_3-symmetry, halogen-bonded network. (e) Optimized parameters of the unit cells for the two assemblies (a) and (c).

6. Statistics of borazatruxene coverage on Au(111)

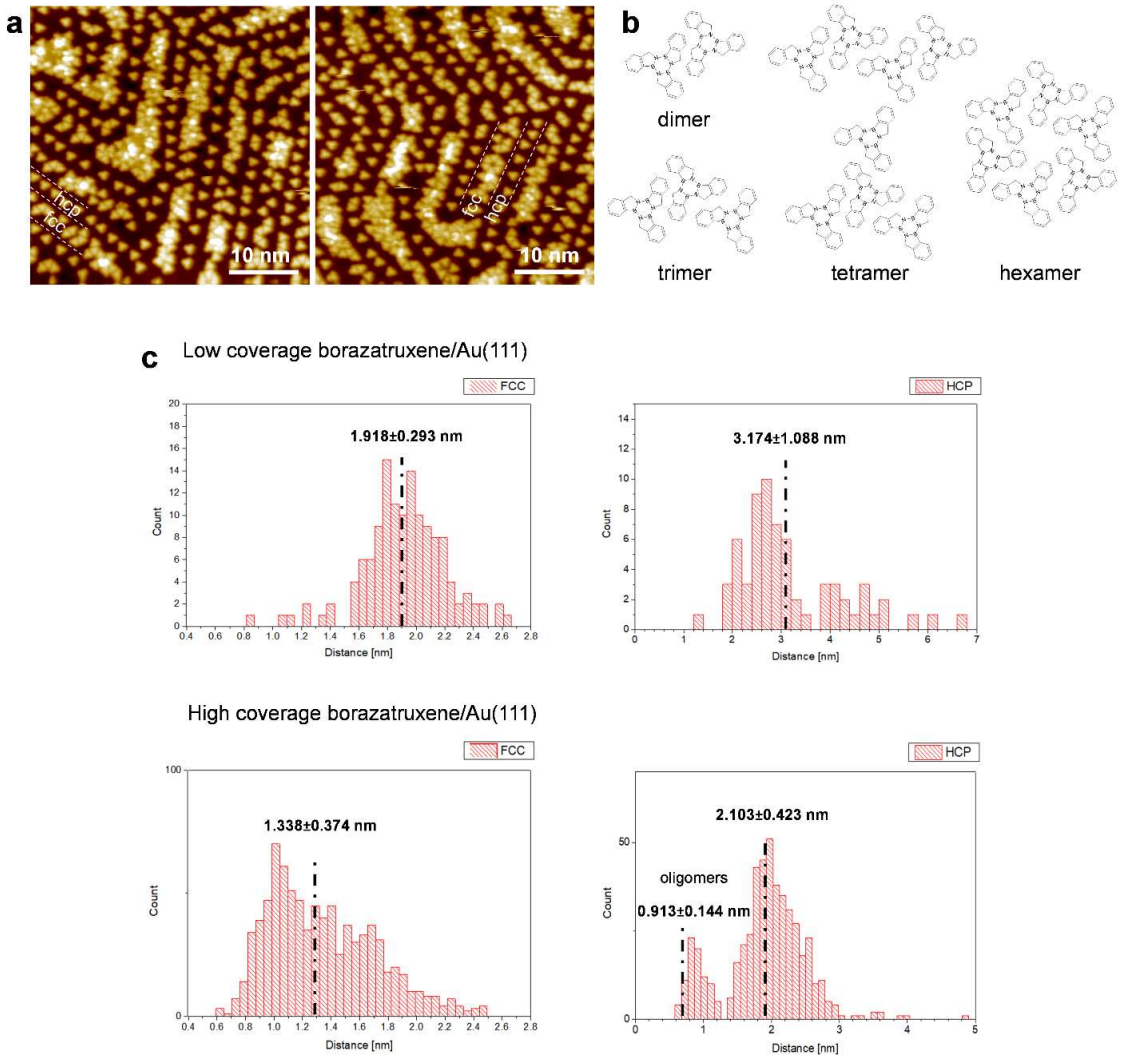

Figure S7. **Nearest-neighbor distance analysis for borazatruxenes on Au(111), for both *fcc* and *hcp* regions, at low and high molecular coverage.** (a) *z* images of borazatruxenes on Au(111) at high molecular coverage show an increase in molecular density in the *fcc* regions, while molecules are still well separated in the *hcp* regions of the substrate. (b) Nearest-neighbor diagrams for low (as in Figure 4a) and high molecular coverage *z* images of borazatruxene on Au(111). The peaks of the pairwise distance distributions yield the average intermolecular distances. The average pair distance decreases with the increase of molecular coverage. At high molecular coverage, several types of assemblies take place on the *hcp* regions, monomers and oligomers, leading to a two-peak distribution.

Figure 4 in the main text showed that at low and intermediary molecular coverage, borazatruxene molecules are isolated and do not form dimers or other higher order structures, the molecular

density being larger on the Au(111) *fcc* regions compared to the *hcp* ones. This difference between the *fcc* and *hcp* regions continues at high (below saturation) molecular coverage; however, in strong contrast with the lower coverages, the intermolecular distances can decrease substantially on both regions, with the occurrence of patches of dimers, trimers, chains and other oligomers. This behavior is reminiscent of that observed in Cheng et al[1]: at low and intermediate coverage, the molecules are isolated, while oligomers form at higher coverage. In our case, we showed in Figure 4e of the main text that the borazatruxenes placed in dimer configuration in vacuum are subjected to repulsive forces (as opposed to attractive forces for 3Br-borazatruxenes), while Figures 4a,b shows that absorption on the Au(111) does not tip the balance of forces towards dimer formation. We posit that at high coverage of borazatruxenes on the Au(111) surface, the interaction with the surface pins the molecules down and is the dominant factor in determining the resulting intermolecular distances.

7. Bader analysis for borazatruxene, 3Br-borazatruxene, and truxene on Au(111)

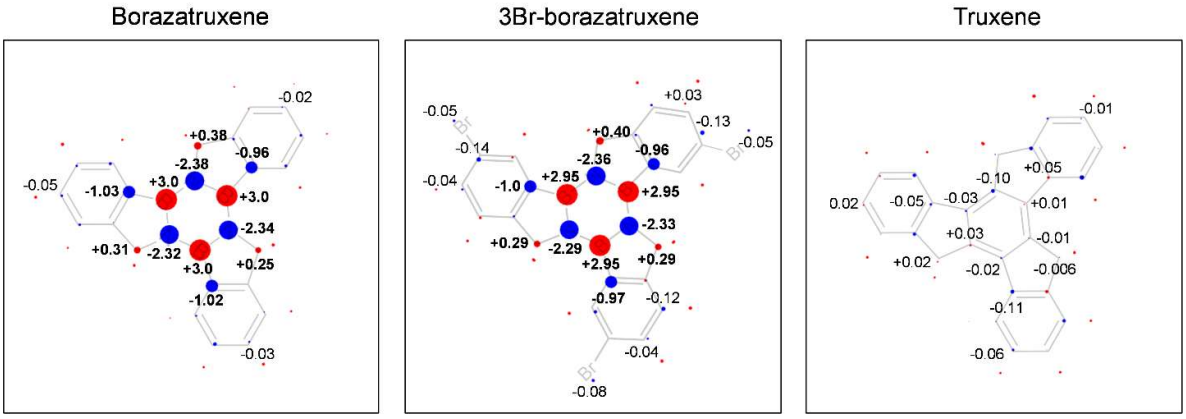

Figure S8. Computed partial charges via Bader analysis (with chemical structures superposed) of the three molecules on Au(111). Size of spheres associated with the atoms are proportional to the value of the partial charge on each atom, while red (blue) indicate positive (negative) partial charge. The substrate is omitted for clarity. For selected sites, the partial charge is also indicated numerically (in units of electron charge), for clarity. The slight asymmetry in charge on equivalent sites of the molecule is due to the placement of the molecule on Au(111).

Using the Bader analysis code[2], partial charges have been computed for each atom of the three precursors adsorbed on a three layer Au(111) slab using the following equation $\Delta q = q_{Bader} - q_{nominal}$, where q_{Bader} represents the calculated Bader atomic charge and $q_{nominal}$ is the charge associated to the valence electrons of each specific atom. The spheres in Figure S7 are proportional to the absolute values of the partial charges, while red (blue) depicts positive (negative) partial charges.

Borazatruxene and 3Br-borazatruxene/Au(111) show strong polar bonds in the BN ring, as well as for the B-C and B-N bonds adjacent to the core, while partial charges on truxene/Au(111) are negligible, which sets a clear distinction in the charge distribution of the two isosteres (truxene and borazatruxene). Thus, for B atoms in the BN ring of borazatruxene/Au(111) the partial charge is +3.0, while for N atoms this is -2.3 (in units of electron charge). The partial charge on the methylene C is +0.3, while for the aromatic C adjacent to B it is -1.0 (in units of electron charge).

8. Borazatruxene: relationship between molecular resonances on Au(111) and molecular states in vacuum

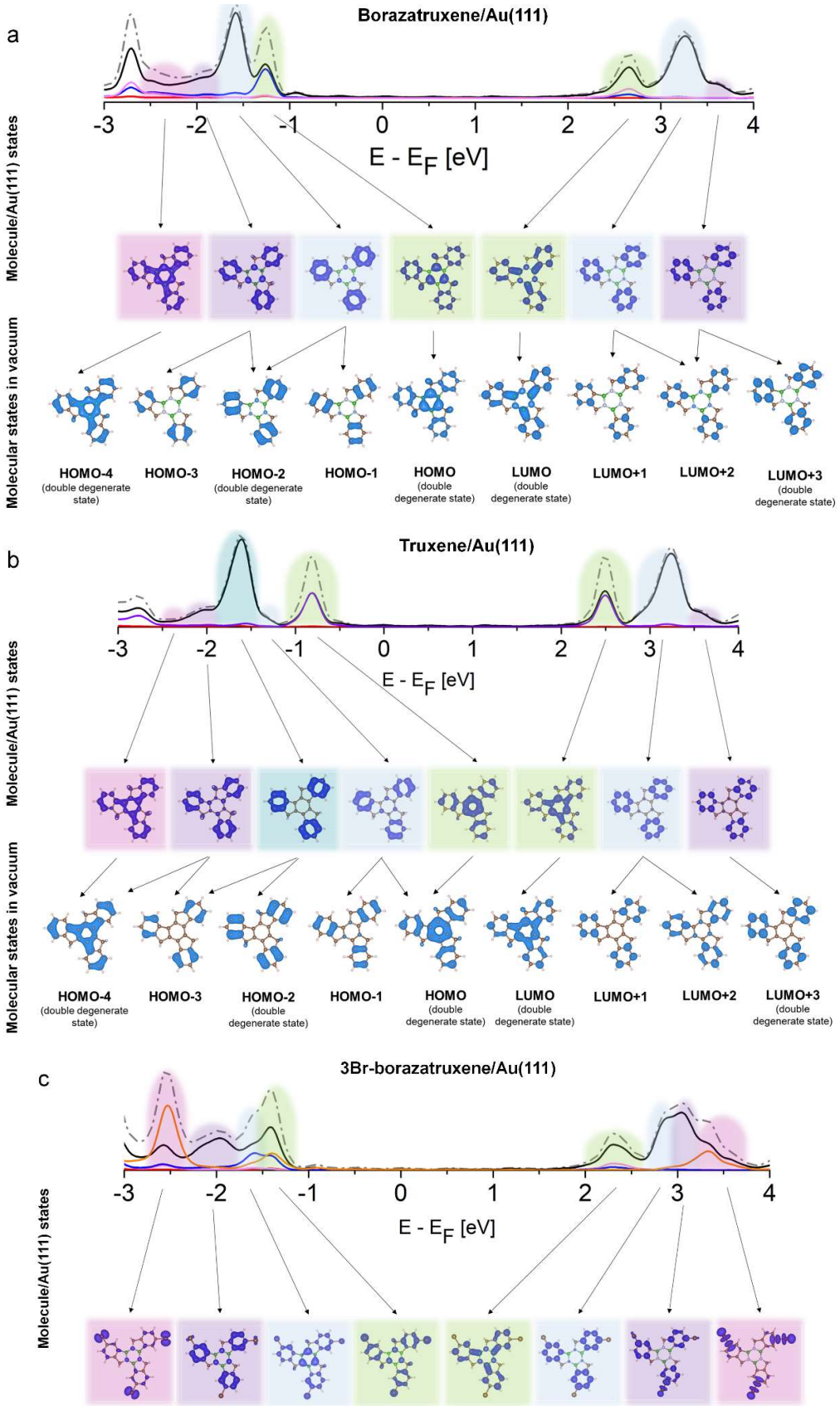

Figure S9 Decomposition of computed molecular resonances of (a) borazatruxene, (b) truxene and (c) 3Br-borazatruxene on Au(111) as a linear superposition of molecular states in vacuum (i.e. LUMO,... LUMO+n, and HOMO,...HOMO-n). Top row: computed projected DoS (pDOS) of the molecule/Au(111) system onto molecular states; middle row: the associated integrated local density of states (ILDOS) maps (plotted at normalized isovalue, see text); bottom row: the dominant molecular states in vacuum contributing to the respective ILDOS map, at selected energies, plotted at 0.0012 e/bohr^3 isovalue.

Projected densities of states (pDOS) plots were obtained by projecting the states of the combined molecule/metal system onto (i) vacuum molecular states (total pDOS) and (ii) atomic orbitals of interest (B, N, C, Br states).

Molecular resonances of the molecule/metal system were identified as peaks in the total pDOS plots. The spatial charge distribution of each molecular resonance was evaluated by integrating the molecular states within their corresponding energy range, yielding the ILDOS (integrated local density of states) maps plotted in the middle row of Figures S8 a and b. The corresponding energy ranges are highlighted in the color corresponding to each ILDOS map. The isovalue for which ILDOS maps were plotted has been normalized to $I_{normalized}$ = 0.0007 e/bohr^3 × Peak Area of each molecular resonance. This is done so that a consistent comparison between maps could be conducted.

The bottom rows of Figures S8a,b show the molecular orbitals of borazatruxene and truxene, respectively, calculated in vacuum. Both molecules have double degenerate frontier orbitals in vacuum; in such cases, the molecular orbitals shown are the equally weighted arithmetic average of the degenerate orbitals.

The existence of doubly-degenerate HOMO and LUMO states for borazatruxene and truxene, combined with their three-fold symmetric geometry, potentially confers on them intriguing optical properties; e.g. photoluminescence anisotropy has been partly studied for truxene-cored molecules[3].

Molecular adsorption on Au(111) leads to energy level broadening and mixing of vacuum molecular states, therefore the molecular resonances on the metallic substrate represent the mixing of vacuum orbitals. The ILDOS maps of the molecular resonances on Au(111) (middle row in Figures S8a,b) were decomposed onto molecular vacuum orbitals (bottom row) and the main orbital contribution to the specific molecular resonances on the metal is shown by the arrows. For example, for borazatruxene/Au(111), the HOMR molecular resonance at -1.26 eV is decomposed onto vacuum wavefunctions (φ) as follows: $\psi = 0.53\,\varphi_{HOMOa} + 0.41\,\varphi_{HOMOb} + 0.17\,\varphi_{HOMO-1} + 0.008\,\varphi_{HOMO-} + \cdots$, where indices *a* and *b* in φ_{HOMOa} and φ_{HOMOb} designate the degenerate wavefunctions of the vacuum HOMO state. Therefore, for this specific state, the arrow points towards the vacuum HOMO double degenerate orbital, which has the greatest contribution.

9. Experimental DOS spectra for borazatruxene molecule on Au(111)

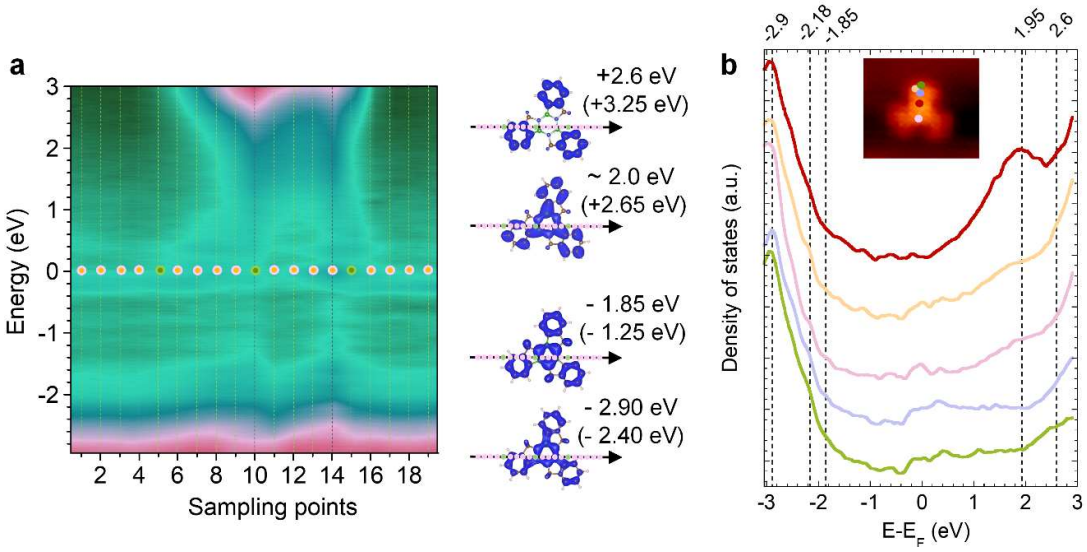

Figure S10 (a) 3D "DOS (Energy) *vs* distance" experimental maps taken along a line scan across a borazatruxene molecule, complementing the data from Figure 5c. The sampling points relative to the molecule position are indicated with pink and green dots along the sampling direction. Right: computed ILDOS maps for selected energies: experimental values for the molecular resonances are downshifted relative to theoretical ones (in brackets) by about 0.6 eV. Sampling direction is indicated by the black arrow. Sampling points 10 and 14 (dark lines) on the LDOS map probe sites in the vicinity of the boron sites of the central borazine ring, where increased charge density is expected based on Figure 5a. **(b) Site-dependent DOS (Energy) for borazatruxene corresponding to the dI/dV spectra shown in Figure 5(b)**, the same color code being used to indicate the sites of the individual spectra. The spectra were staggered on the *Oy* axis for ease of viewing. For both (a) and (b), the DOS (Energy) spectra were obtained from the dI/dV (bias voltage) spectra using a deconvolution procedure detailed in Wagner et al[4] that eliminates the bias-dependent barrier transmission function.

10. Conformation of borazatruxene, 3Br-borazatruxene and truxene on Au(111)

	Borazatruxene	3Br-borazatruxene	Truxene
B	3.363249	3.373037	
N	3.378708	3.385761	
core	3.370978	3.379399	3.370276
C_m	3.385413	3.404079	3.395830
C_1	3.358017	3.413119	3.371002
C_2	3.311564	3.396712	3.319766
C_3	3.2531	3.35124	3.262269
C_4	3.241846	3.330394	3.255306
C_5	3.28527	3.345348	3.301361
C_6	3.342609	3.387838	3.357811
ar H or Br	3.203948	3.184604	3.196474
methylene H_1	2.49492	2.500799	2.518018
methylene H_2	4.269981	4.275974	4.282643
Angle between core and aromatic rings	2.51°	1.76°	2.55°
Molecular dipole in z direction	-0.17D	-0.08D	-0.15D

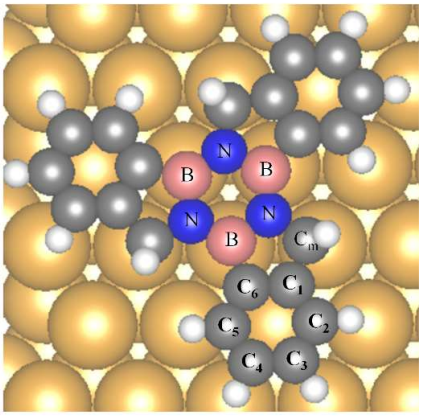

Figure S11. **Optimized molecular conformation of borazatruxene, truxene and 3Br-borazatruxene on a three-layer Au slab calculated at PBE+D3 level.** Molecule-substrate distances for optimized geometries, together with angles between BN or C molecular core (for truxene) and outer aromatic ring planes. Computed molecular dipole in the z direction, due to bending when adsorbed on the substrate, is also included.

11. Experimental differential conductance maps and DOS spectra for individual molecules of borazatruxene, 3Br-borazatruxene and truxene

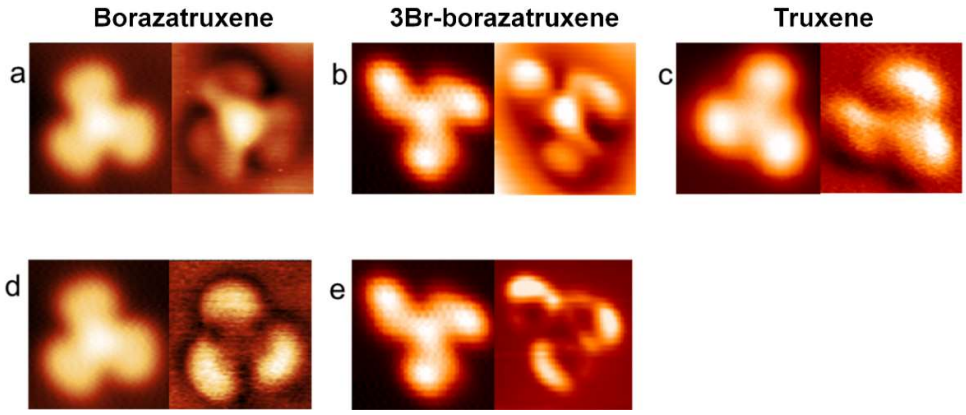

Figure S12. **Constant current experimental dI/dV maps for borazatruxene, 3Br-borazatruxene, and truxene on Au(111).** Tunneling parameters: (a) -3.1 V, 6 nA (b) -3.2V, 6.2 nA , (c) -3 V ,4.8 nA, (d) -2.5 V, 6 nA and (e) -2.2V, 2.3 nA. For each set of images, z (topographic) image at left, and dI/dV image at right. The choice of tunneling conditions is consistent with Figure 6 (main text) and justified in Methods.

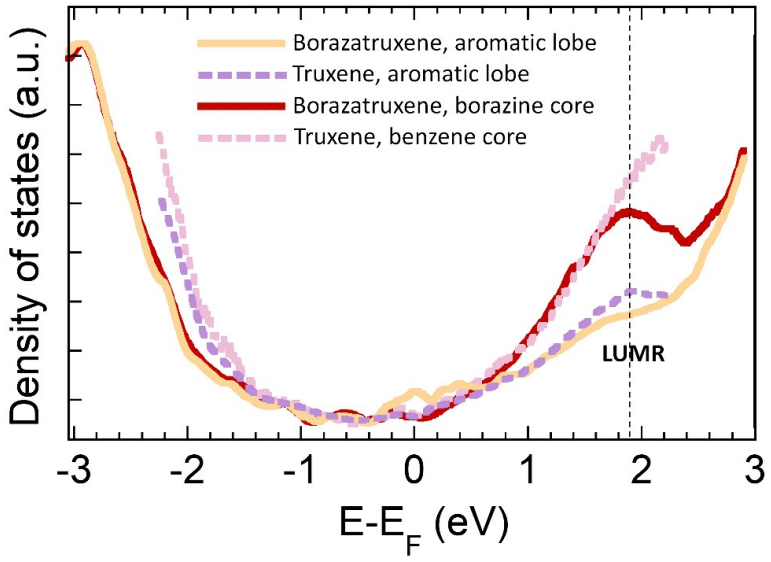

Figure S13. **Site-dependent experimental DOS (Energy) spectra for borazatruxene *vs.* truxene molecules on Au(111)**. The DOS (Energy) spectra were obtained from dI/dV (bias voltage) spectra using a deconvolution procedure detailed in Wagner et al[4] that eliminates the bias-dependent barrier transmission function: borazatruxene, full lines; truxene, dotted lines. The spectra for borazatruxene are from the set shown in Figure S10b. The state at ~ 1.9-2eV is assigned to LUMR as it is expected to be seen both above cores and aromatic lobes, for both molecules. The identification of this state allowed for the truxene and borazatruxene spectra taken above the aromatic lobes – a common functional group for both molecules – to be normalized

to each other at the LUMR state. This procedure then allowed for the occupied states, below the Fermi energy of the two molecules, to be compared: despite the lower quality of the truxene spectra, the molecular gap for truxene can be seen to narrow significantly compared to borazatruxene as the HOMR states for truxene are located at higher energy, as expected from the PDOS simulations in Figure 5a (main text).

12. Band structure of the low symmetry, 3Br-borazatruxene 2D network, its doping with atomic Na and anisotropy characteristics

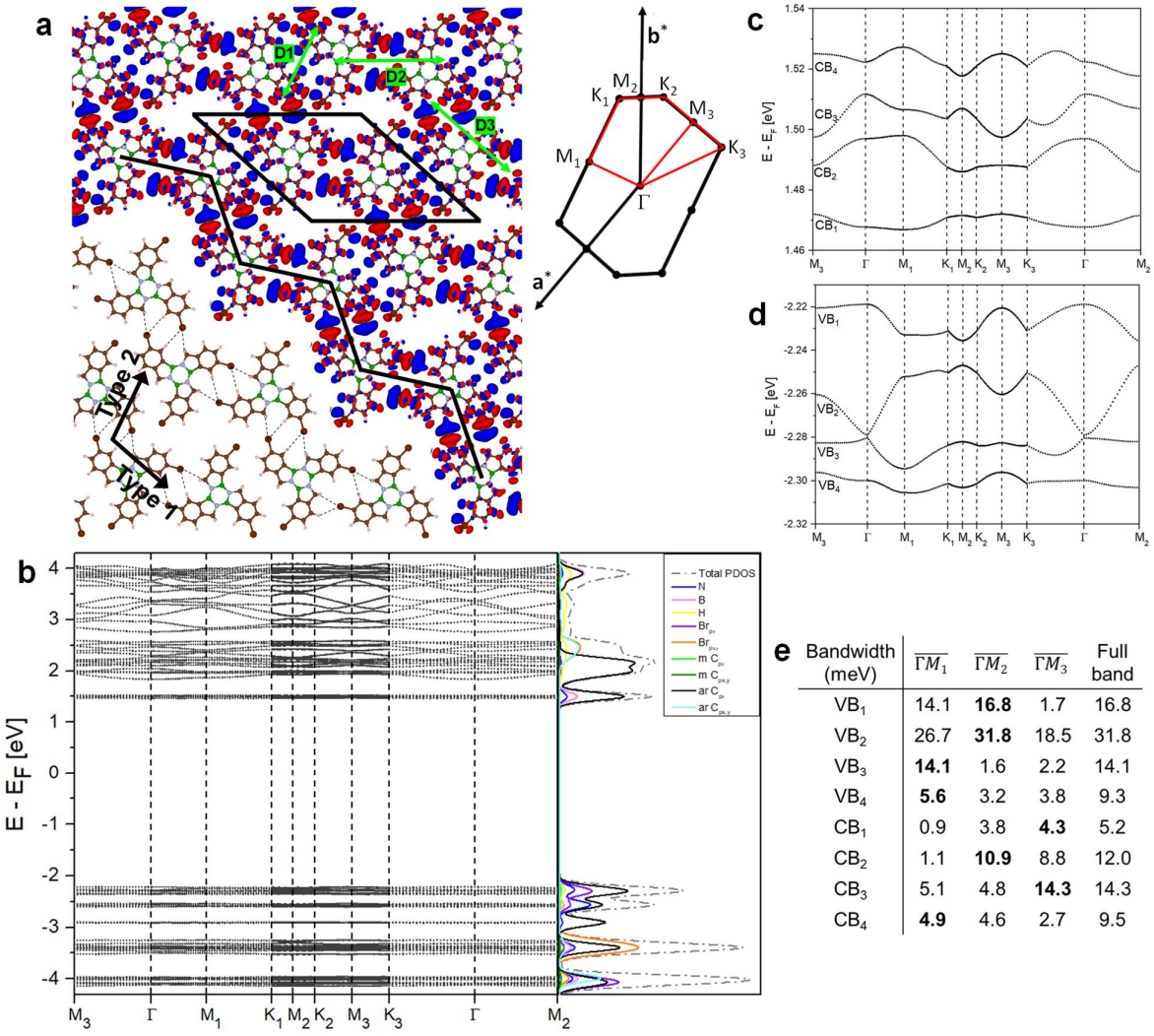

e

Bandwidth (meV)	$\overline{\Gamma M_1}$	$\overline{\Gamma M_2}$	$\overline{\Gamma M_3}$	Full band
VB_1	14.1	**16.8**	1.7	16.8
VB_2	26.7	**31.8**	18.5	31.8
VB_3	**14.1**	1.6	2.2	14.1
VB_4	**5.6**	3.2	3.8	9.3
CB_1	0.9	3.8	**4.3**	5.2
CB_2	1.1	**10.9**	8.8	12.0
CB_3	5.1	4.8	**14.3**	14.3
CB_4	**4.9**	4.6	2.7	9.5

Figure S14 DFT-calculated band-structure of the low-symmetry, 3Br-borazatruxene H-bonded 2D network. (a) Charge density difference (CDD) map showing the type 1 and 2 homodimer-based chain directions and the three crystallographic axes of the 2D crystal, D_1 to D_3 (in green). Also shown are the real space unit cell vectors and the calculated ***k***-paths within the first Brillouin zone (in red). (b) Band-structure calculated along the highlighted ***k***-paths and corresponding orbital-projected density of states (pDOS). Total DOS is in grey, while the atomic contributions are color coded: N, blue; B, pink; H, yellow; Br_{p_z}, purple; $\mathrm{Br}_{p_{x,y}}$, orange; methylene C_{p_z} and $C_{p_{x,y}}$, light and dark green, respectively; aromatic C_{p_z} and $C_{p_{x,y}}$, black and cyan, respectively. (c-d) Zoom into the four frontier conduction $CB_{1\text{-}4}$ and valence bands $VB_{1\text{-}4}$, respectively. (e) Bandwidths (BW) for $VB_{1\text{-}4}$ and $CB_{1\text{-}4}$ calculated along ΓM_1, ΓM_2 and ΓM_3, corresponding to the three

crystallographic directions D1 to D3; the largest bandwidth is shown in bold. BWs for the entire bands are also shown.

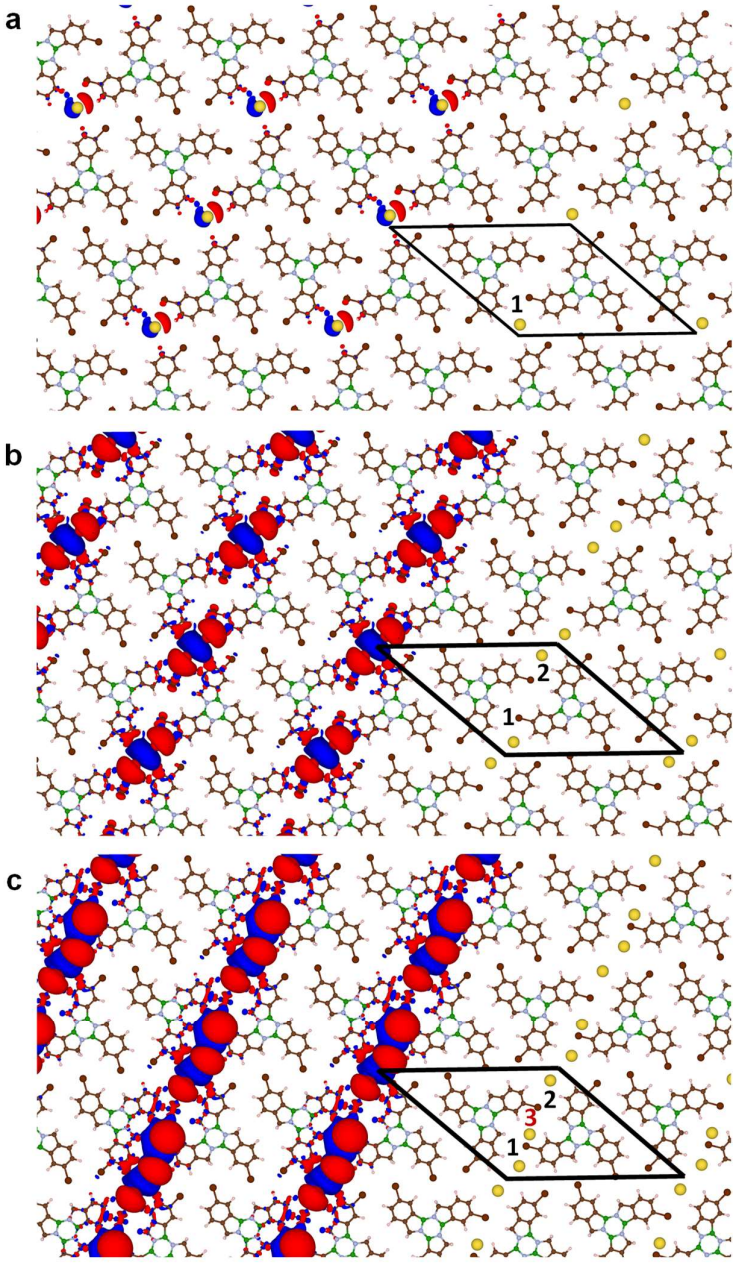

d

	Binding energy to other dopants and 2D network (eV)	Δz of Na atoms relative to the average z of 2D network plane (Å)
1 Na atom / unit cell	-0.246	Δz_1 = 1.93
2 Na atoms / unit cell	-1.074	Δz_1 = 2.07 Δz_2 =1.99
3 Na atoms / unit cell	-1.528	Δz_1 = 2.75 Δz_2 = 1.92 Δz_3 = 3.29

Figure S15 Atomic Na pore trapping and adsorption on the low symmetry, 3Br-borazatruxene 2D network. DFT-optimized structures and charge density difference (CDD) maps, $\Delta\rho(r) = \rho_{network+nNa\ atoms} - \rho_{network} - \sum_{i=1}^{n} \rho_{Na_i\ atoms}$, where n is the total number of Na atoms for each case. For (a) one pore-trapped Na atom, (b) two pore-trapped Na atoms, and (c) three Na atoms, two trapped inside pores (numbered as 1

and 2, in black) and a third adsorbed on an energetically preferred network site (numbered as 3, in red). CDD maps are plotted for (a) $\Delta\rho(r)$=0.0015 e/bohr^3 and (b-c) $\Delta\rho(r)$=0.003 e/bohr^3 isovalues; excess of electrons, blue; deficit of electrons, red. (d) Total binding energies of the Na atoms when trapped/adsorbed on the network, $E_{binding}$, and their z distances to the plane of the molecular network for cases (a-c).

$E_{binding}$, the total binding energy of the *n* Na atoms/unit cell when adsorbed on the 2D network was calculated as:

$$E_{binding} = E_{network+nN} - E_{network} - \sum_{i=1}^{n} E_{Na_i}. \quad (1)$$

where energies for the undoped network, $E_{network}$, and those for the individual Na atoms in the optimised, network-adsorbed configurations, E_{Na_i}, are subtracted from the total energy of the compound, doped system (i.e. network with the *n* Na dopant atoms in the optimised adsorption geometry), $E_{network+nNa}$.

$E_{binding}$ can also be seen as having two components: (i) the energy of binding the *n* Na dopants to the 2D network, $E_{bind\_nNa\_to\_network}$, and (ii) the interaction energy between the dopants themselves, E_{bind_nNa}:

$$E_{binding} = E_{bind\_nNa\_to\_network} + E_{bind\_nNa}. \quad (2)$$

The $E_{bind\_nNa\_to\_network}$ term is obtained as:

$$E_{bind\_nNa\_to\_2D} = E_{network+nN} - E_{network} - E_{nNa} \quad (3)$$

where E_{nNa} is the total energy of the group of interacting dopants in the optimized adsorption configurations on the network, obtained from the compound system when the network component is removed.

The interaction energy between the dopants themselves, E_{bind_nNa} is obtained as:

$$E_{bind\_nNa} = E_{nNa} - \sum_{i=1}^{n} E_{Na_i}. \quad (4)$$

Substituting equations (3) and (4) in equation (2), equation (1) is obtained, demonstrating that the definitions are consistent with each other.

These definitions are also used for calculating the energy terms from Figure S18.

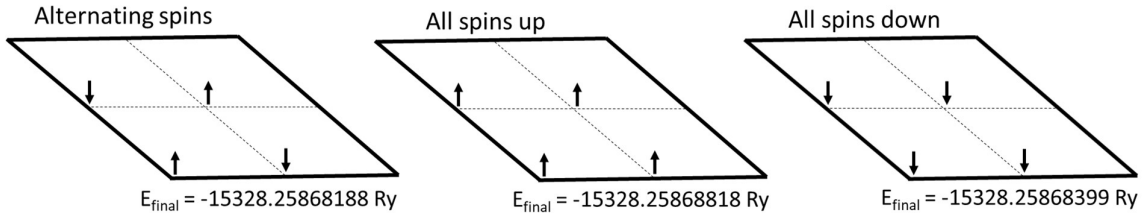

Figure S16 Trapping of one Na atom in the pores of the low symmetry, 3Br-borazatruxene 2D network: comparison of total energies for various spin configurations. Atomic configuration corresponds to Figure S15(a). The final energy was computed at the PBE+D3/PAW level for three spin configurations, where the Na atoms' magnetization was fixed in certain directions: (i) alternating spins, (ii) all spins up, and (iii) all spins down. These configurations were chosen with the aim of testing whether any long-range Na spin interactions can develop in this system. The three spin configurations differ by less than 1 meV, which implies that there

is no preferred spin configuration of the Na atoms, hence the network with one trapped Na atom is paramagnetic.

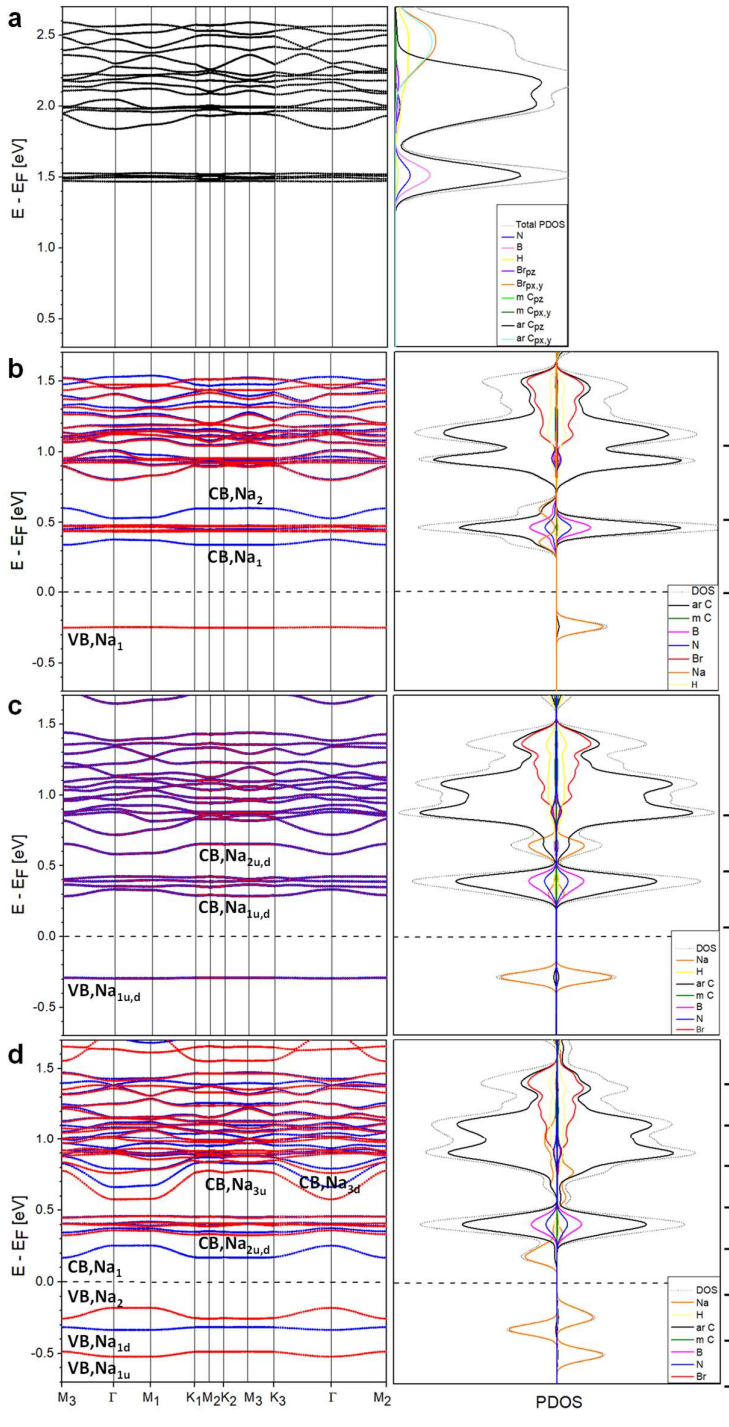

Bandwidth (meV)	$\overline{\Gamma M_1}$	$\overline{\Gamma M_2}$	$\overline{\Gamma M_3}$	Full band
VB,Na_1	0.2	3.3	3.4	3.4
CB,Na_1	4.8	35.8	37.5	37.5
CB,Na_2	5.3	70	71.3	71.3

Bandwidth (meV)	$\overline{\Gamma M_1}$	$\overline{\Gamma M_2}$	$\overline{\Gamma M_3}$	Full band
VB,$Na_{1u,d}$	0.1	4.9	4.8	4.9
CB,$Na_{1u,d}$	4.3	40	47.3	47.3
CB,$Na_{2u,d}$	7.4	71.6	72.3	72.3

Bandwidth (meV)	$\overline{\Gamma M_1}$	$\overline{\Gamma M_2}$	$\overline{\Gamma M_3}$	Full band
VB,Na_{1u}	0	43.4	43.4	43.4
VB,Na_{1d}	0	18.8	18.8	18.8
VB,Na_2	0	93.8	94.3	94.3
CB,Na_1	1	101	101.3	101.3
CB,Na_{2u}	2.1	24.8	33	33
CB,Na_{2d}	2.1	21.6	31.5	31.5
CB,Na_{3u}	0.6	212.5	207.7	212.5
CB,Na_{3d}	7.9	179.4	171.3	179.4

Figure S17 Band-structure of atomic Na-doped, low-symmetry, 3Br-borazatruxene 2D network. Na atoms are pore-trapped and adsorbed, respectively. Blue and red relate to the two spin orientations. Atomic orbital-projected density of states (pDOS), as well as bandwidths of the Na-related hybrid bands are shown. The ***k***-paths match those described in Figure S14. (a) Comparison with undoped 3Br-borazatruxene network, for relevant bands. (b-c) Pore trapping of one and two Na atoms, respectively, corresponding to Figure S15(a-

b). (d) Adsorption of a third atom on an energetically preferred network site, corresponding to Figure S15(c). For pDOS, atomic contributions are color-coded: N, blue; B, pink; H, yellow; aromatic C, black; methylene C, green; Br, red and Na in orange; total DOS is in grey. In all cases, there is substantial Fermi level shift compared to the undoped lattice. Na-related hybrid bands acquire anisotropic dispersion, with bandwidths shown in tables.

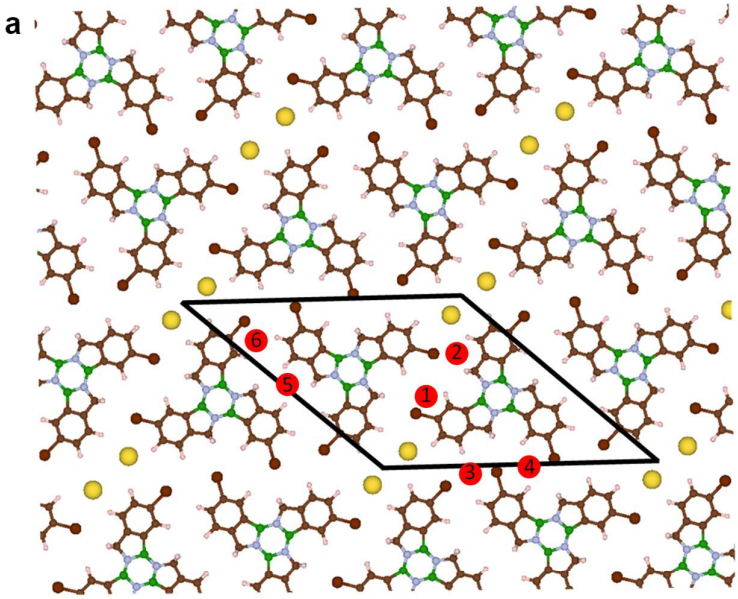

b	Binding energy of the n Na atoms to the 2D network $E_{bind\_nNa\_to\_network} = E_{network+nNa} - E_{network} - E_{nNa}$ (eV)	Inter-dopant binding energy $E_{bind\_nNa} = E_{nNa} - \sum_{i=1}^{n} E_{Na_i}$ (eV)	Binding energy to 2D network and other dopants $E_{bind\_nNa\_to\_network} + E_{bind\_nNa}$ (eV)	Δz of Na atoms relative to the average z of 2D network plane (Å)
1 Na atom / unit cell	-0.246			Δz_1 = 1.93
2 Na atoms / unit cell	-0.559	-0.515	-1.074	Δz_1 = 2.07 Δz_2 =1.99
3 Na atoms / unit cell: configuration 1	-0.670	-0.858	-1.528	Δz_1 = 2.75 Δz_2 = 1.92 Δz_3 = 3.29
3 Na atoms / unit cell: configuration 2	-0.448	-0.913	-1.361	Δz_1 = 2.04 Δz_2 = 2.21 Δz_3 = 3.60
3 Na atoms / unit cell: configuration 3	-0.722	-0.850	-1.572	Δz_1 = 2.33 Δz_2 = 2.04 Δz_3 = 3.07
3 Na atoms / unit cell: configuration 4	-0.865	-0.520	-1.385	Δz_1 = 2.04 Δz_2 = 2.00 Δz_3 = 3.05
3 Na atoms / unit cell: configuration 5	-0.758	-0.520	-1.278	Δz_1 = 2.07 Δz_2 = 2.00 Δz_3 = 3.07
3 Na atoms / unit cell: configuration 6	-0.634	-0.853	-1.487	Δz_1 = 2.80 Δz_2 = 1.95 Δz_3 = 3.25

Figure S18 Binding energy for up to three Na atoms per unit cell on the low symmetry, 3Br-borazatruxene 2D network: total binding energy and contributing components. Yellow-colored atoms are pore-trapped as

in Figure S15, while the third atom is adsorbed on various un-equivalent sites, 1 to 6, in the unit cell, as marked by red circles in (a). (b) The total binding energy of the *n* atoms/unit cell, $E_{binding}$, shown in the 3rd column, has contributions from the *n* Na atom interaction with the 2D network $E_{bind\_nNa\_to\_network}$ (column 1) and with themselves E_{bind_nNa} (column 2). The Na atoms' distances to the average plane of the 2D network, Δz, are also shown: pore-trapped atoms have a significantly lower Δz compared to the third Na atom, which is merely adsorbed on lattice sites.

The energies listed in Figure S18b are defined and calculated as in Figure S15.

We now discuss some general trends revealed by the binding energy terms:

For the 3 Na atoms/unit cell system, configurations 1, 3 and 6 yield the largest total binding energies and are, hence, favored. The inter-dopant binding energy E_{bind_nNa} is largest as a result of the proximity of the three atoms in these geometries. The larger Δz values for the pore-trapped and adsorbed atoms allow for a stronger interaction between the three Na atoms, while weakening the binding to the 2D network as reflected by the lower values of $E_{bind\_nNa\_to\_network}$ compared to the remaining configurations 2, 4 and 5.

For configurations 2, 4 and 5, E_{bind_nNa} is lower than for 1, 3, and 6, as the third, adsorbed atom is well distanced from the pore-adsorbed atoms. This also leads to lower values of Δz to the average plane of the 2D network, which in turn increases the binding of the dopant atoms to the network, $E_{bind\_nNa\_to\_network}$.

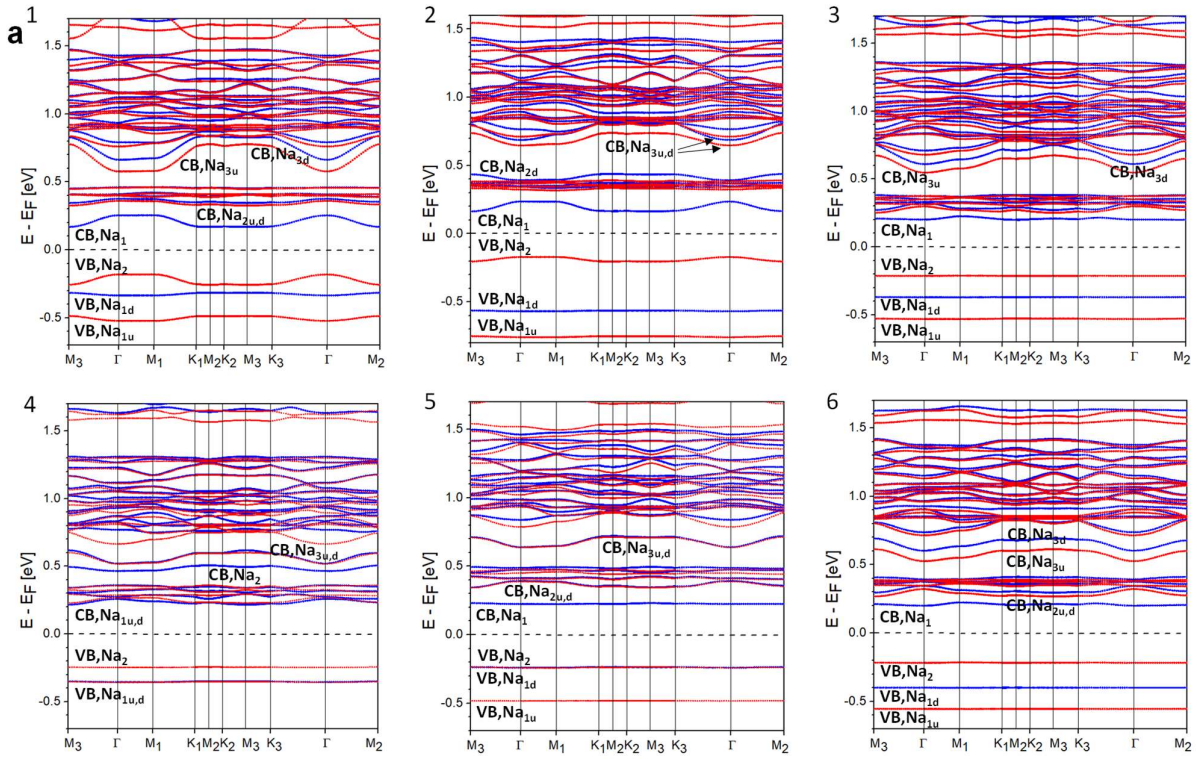

b Configuration 1

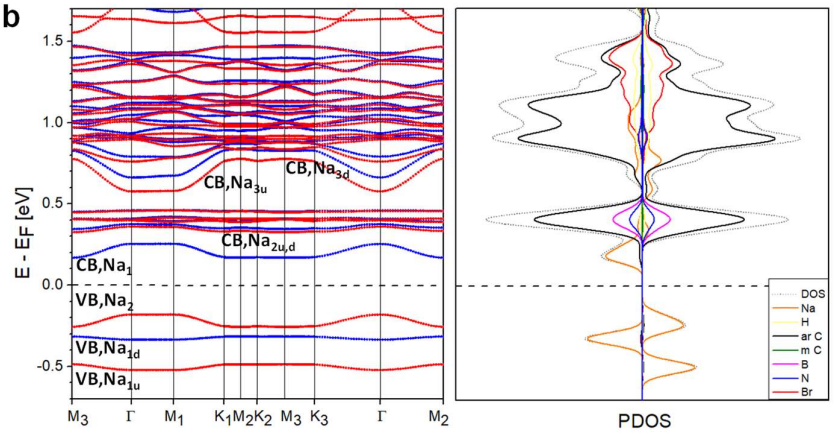

Bandwidth (meV)	$\overline{\Gamma M_1}$	$\overline{\Gamma M_2}$	$\overline{\Gamma M_3}$	Full band
VB,Na_{1u}	0	43.4	43.4	43.4
VB,Na_{1d}	0	18.8	18.8	18.8
VB,Na_2	0	93.8	94.3	94.3
CB,Na_1	1	101	101.3	101.3
CB,Na_{2u}	2.1	24.8	33	33
CB,Na_{2d}	2.1	21.6	31.5	31.5
CB,Na_{3u}	0.6	212.5	207.7	212.5
CB,Na_{3d}	7.9	179.4	171.3	179.4

c Configuration 2

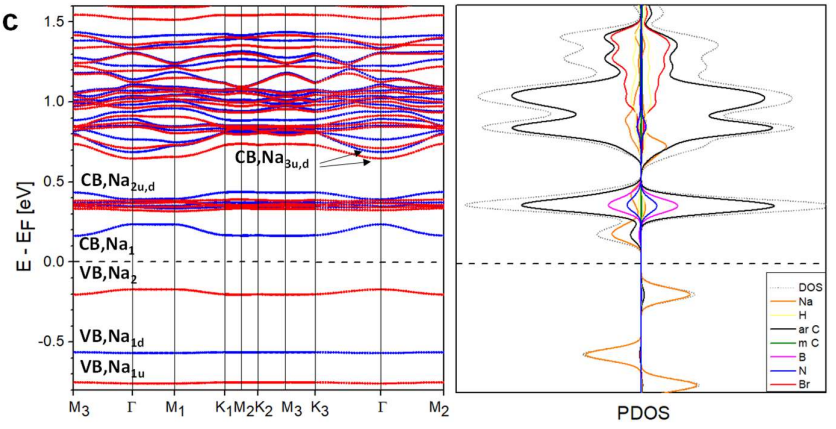

Bandwidth (meV)	$\overline{\Gamma M_1}$	$\overline{\Gamma M_2}$	$\overline{\Gamma M_3}$	Full band
VB,Na_{1u}	0	7.3	7.4	7.4
VB,Na_{1d}	0	5.5	5.4	5.5
VB,Na_2	0.1	32.3	32.5	32.5
CB,Na_1	0.9	70.1	71.6	71.6
CB,Na_{2u}	1.1	5.1	3.1	5.1
CB,Na_{2d}	3	45.1	42.2	45.1
CB,Na_{3u}	10.3	91.6	90.4	91.6
CB,Na_{3d}	39.4	120.9	115.9	120.9

d Configuration 3

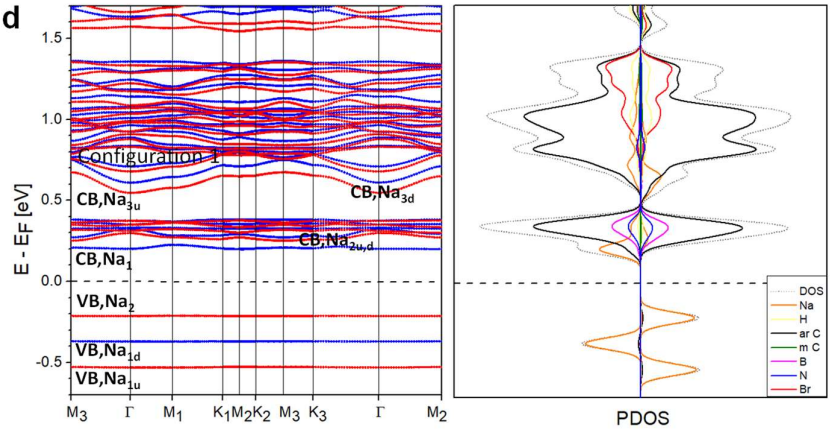

Bandwidth (meV)	$\overline{\Gamma M_1}$	$\overline{\Gamma M_2}$	$\overline{\Gamma M_3}$	Full band
VB,Na_{1u}	0.4	2.6	2.7	2.7
VB,Na_{1d}	0.3	1.9	1.9	1.9
VB,Na_2	2	0.2	0.4	2
CB,Na_1	24.3	2.5	6.5	24.3
CB,Na_{2u}	25.6	26.6	46.2	46.2
CB,Na_{2d}	41	31.2	52.1	52.1
CB,Na_{3u}	30.4	102.5	126.5	126.5
CB,Na_{3d}	34.5	100.9	140.4	140.4

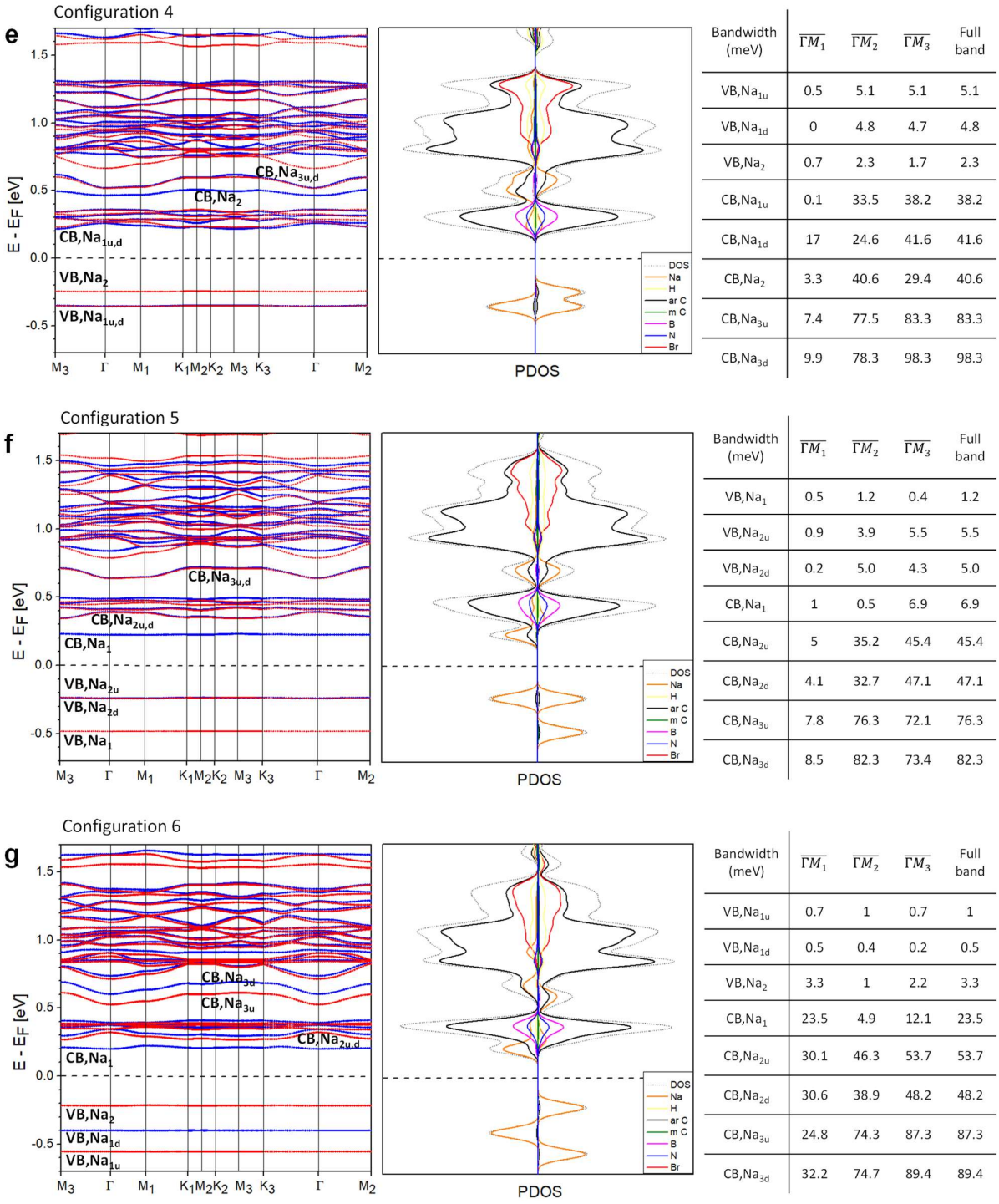

Bandwidth (meV)	$\overline{\Gamma M_1}$	$\overline{\Gamma M_2}$	$\overline{\Gamma M_3}$	Full band
VB,Na_{1u}	0.5	5.1	5.1	5.1
VB,Na_{1d}	0	4.8	4.7	4.8
VB,Na_2	0.7	2.3	1.7	2.3
CB,Na_{1u}	0.1	33.5	38.2	38.2
CB,Na_{1d}	17	24.6	41.6	41.6
CB,Na_2	3.3	40.6	29.4	40.6
CB,Na_{3u}	7.4	77.5	83.3	83.3
CB,Na_{3d}	9.9	78.3	98.3	98.3

Bandwidth (meV)	$\overline{\Gamma M_1}$	$\overline{\Gamma M_2}$	$\overline{\Gamma M_3}$	Full band
VB,Na_1	0.5	1.2	0.4	1.2
VB,Na_{2u}	0.9	3.9	5.5	5.5
VB,Na_{2d}	0.2	5.0	4.3	5.0
CB,Na_1	1	0.5	6.9	6.9
CB,Na_{2u}	5	35.2	45.4	45.4
CB,Na_{2d}	4.1	32.7	47.1	47.1
CB,Na_{3u}	7.8	76.3	72.1	76.3
CB,Na_{3d}	8.5	82.3	73.4	82.3

Bandwidth (meV)	$\overline{\Gamma M_1}$	$\overline{\Gamma M_2}$	$\overline{\Gamma M_3}$	Full band
VB,Na_{1u}	0.7	1	0.7	1
VB,Na_{1d}	0.5	0.4	0.2	0.5
VB,Na_2	3.3	1	2.2	3.3
CB,Na_1	23.5	4.9	12.1	23.5
CB,Na_{2u}	30.1	46.3	53.7	53.7
CB,Na_{2d}	30.6	38.9	48.2	48.2
CB,Na_{3u}	24.8	74.3	87.3	87.3
CB,Na_{3d}	32.2	74.7	89.4	89.4

Figure S19 Band-structure of the low-symmetry, 3Br-borazatruxene 2D network doped with three Na atoms per unit cell: two Na atoms are pore-trapped while the third is adsorbed on various un-equivalent network sites. (a) Comparison of bands relevant to electron transport for 6 non-equivalent Na adsorption sites, configurations labelled 1 to 6. (b-g) Central panels: pDOS contributions (atom colour-coded) for each of the six adsorptions sites of the 3rd Na atom. Right panels: bandwidths of the Na-related bands on the main ***k***-paths in the unit cell. The selection of the ***k***-paths corresponds to Figure S14.

All configurations analyzed in Figure S19 provide bands that can support anisotropic transport, with various, but useful, degrees of energy dispersion. Among them, configurations 1 and 3 are the most

stable energetically. Configuration 1 is the most interesting case, with several Na-network hybrid bands with bandwidths in the 100 to 200 meV range, i.e. VB,Na_2, CB,Na_1, CB,Na_{3u} and CN,Na_{3d}. The effects corresponding to configuration 3 are less strong, however, CB,Na_{3u} and CN,Na_{3d} bands have bandwidths larger than 100 meV.

13. Supramolecular, BN-driven polar interactions: adsorption of borazines in staggered *vs* eclipsed configurations

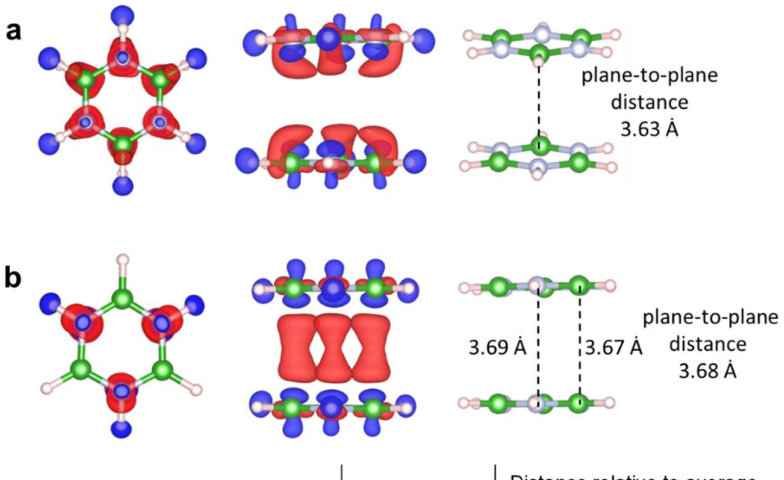

c

	Binding energy (eV)	Distance relative to average 2D network plane (Å)
2D network - borazine, eclipsed	-0.298	3.63
2D network - borazine, staggered	-0.398	3.44
borazine – borazine, eclipsed	-0.092	3.68
borazine – borazine, staggered	-0.149	3.63

Figure S20 Stacking of borazine dimers: staggered *vs* eclipsed. Optimized geometry parameters and charge density difference (CDD) maps for (a) staggered and (b) eclipsed configurations. $\Delta\rho(r) = \rho_{stacked\_dimers} - \sum_{i=1}^{2} \rho_{borazine_i}$ plotted for 0.00015 e/bohr^3 isovalue: excess of electrons, blue; deficit of electrons, red. (c) Comparison between the binding energies and z distances between the stacked borazines. The binding energy has been computed via $E_{binding} = E_{stacked\_dimer} - \sum_{i=1}^{2} E_{borazine_i}$. At PBE+D3/PAW theory level, the binding energy of stacked dimers calculated for the borazine-borazine stacked dimers is in good agreement with the literature[5]. (c) also lists the binding energy of borazine adsorbed on the 3Br-borazatruxene H-bonded 2D network, in staggered *vs* eclipsed configurations relative to the borazine core of 3Br-borazatruxene. Though borazines bind substantially more strongly to the 3Br-borazatruxene network compared to just other borazines (due to additional interactions between the out-of-plane methylene H atoms and the H atoms of the B-H bonds), the trend remains: the staggered configuration is more strongly bound than the eclipsed one.

1. Cheng, Z. H.; Gao, L.; Deng, Z. T.; Jiang, N.; Liu, Q.; Shi, D. X.; Du, S. X.; Guo, H. M.; Gao, H. J., Adsorption behavior of iron phthalocyanine on Au(111) surface at submonolayer coverage. *J Phys Chem C* **2007,** *111* (26), 9240-9244.
2. Tang, W.; Sanville, E.; Henkelman, G., A grid-based Bader analysis algorithm without lattice bias. *J Phys-Condens Mat* **2009,** *21* (8).

3. Goubard, F.; Dumur, F., Truxene: a promising scaffold for future materials. *Rsc Adv* **2015,** *5* (5), 3521-3551.
4. Wagner, C.; Franke, R.; Fritz, T., Evaluation of I(V) curves in scanning tunneling spectroscopy of organic nanolayers. *Phys Rev B* **2007,** *75* (23).
5. Malenov, D. P.; Aladic, A. J.; Zaric, S. D., Stacking interactions of borazine: important stacking at large horizontal displacements and dihydrogen bonding governed by electrostatic potentials of borazine. *Phys Chem Chem Phys* **2019,** *21* (44), 24554-24564.